

**Progress Toward Microwave Near-Field Manipulation of Micro-Objects**

**Stephen Rosene**

A thesis submitted in partial fulfillment of the requirement for the degree of  
Bachelor of Science in Physics from William Mary

Williamsburg, VA

May 2022

## Abstract

Microwave atom chips are currently being developed for use in manipulating ultracold atoms, but they may also be useful for manipulating small macroscopic objects. An alternating magnetic field will exert a force on ring-like micro-objects with a self-inductance. One candidate object is a microring which capitalizes on the self-inductance of a torus.

This project pursued two parallel research directions. First, experiments were conducted using macroscopic objects (multi centimeter scale) to verify theoretical predictions. Second, the substrates for the microwave tweezer were developed and characterized.

For the macroscopic experiments research thrust, first an experiment was attempted to measure the force of an alternating B-field on a ring. A wire ring was set up in a pendulum that would be sensitive to a small electromagnetic force. Second, an experiment was conducted to verify that the current varied with frequency from resistive to inductive behavior.

For chip development, first copper substrate candidates were produced through polishing. Second, the properties of a custom commercially produced copper substrate with an aluminum nitride coating were measured. Finally, simulations were conducted to inform the design of a microstrip based microwave cavity for determining the dielectric constant and loss tangent.

# Chapter 1

## Introduction

### 1.1 Motivation

The long term purpose of this project is the development of "microwave tweezer" chips for the manipulation of micro-objects. The primary micro-object that the tweezers will manipulate are aluminum microrings, 50 microns across, developed by our partners at Virginia Commonwealth University (see figure 1).



Figure 1.1: Aluminum Microrings - Manufactured by David Pate at VCU

The development of these microwave tweezer chips has two motivations: the direct benefits of microwave tweezer applications, and the indirect benefits gained from learning manufacturing principles that will be applied to the atom chip and eventually the atom interferometer.

One of the direct benefits of electromagnetic manipulation of macroscopic objects could be in microfluidics. Electromagnetically manipulated rings could be used to

manipulate fluids inside of micro-channels without having to disrupt the channel. Microfluidics itself has applications in biochemistry and nanotechnology.

In terms of indirect benefits, working on the microwave tweezer chips has been an effective way to develop the lab's manufacturing proficiency. Through this process the lab has identified the best strategies to manufacture materials and has developed procedures to test materials for required properties.

## 1.2 Objective and Progress

To advance the development of the microwave tweezer chip, two parallel project paths were carried out. Macroscopic experiments were carried out to verify that the microwave tweezer design would work as expected. At the same time, progress was made toward the manufacturing of the chip itself by creating and analyzing substrate materials and by designing microstrip transmission lines for the chips.

For the macroscopic experiments an attempt was made to measure the force predicted by theory. Next the relationship between the frequency of an alternating magnetic field and the current it induces was examined.

For the manufacturing process three substrate candidates were investigated. The first substrate investigated were copper pieces cut and polished in the lab. The second substrate was manufactured by, CERcuits LLC, a third party manufacturer and tested in the lab to determine plerarity and thickness. Design work was also done to create a chip to test the properties of this substrate. The third candidate was manufactured by Nitride Global LLC, another third party manufacturer. Tests were done to access the thickness of the aluminum nitride layer. In addition, a micro-cavity chip was designed to access the dielectric constant and loss of the aluminum nitride material.

# Chapter 2

## Theory

This chapter presents the basic theory that makes magnetic manipulation of micro-objects possible.

### 2.1 Electromagnetic Properties of a Loop in a B-Field

#### 2.1.1 Current Induced in a Conducting Loop

Let us model the situation where a conducting loop with both resistance  $R$  and an inductance  $L$  is subject to an alternating magnetic field  $B = B_0 \cos(\omega t)$  where  $\omega = 2\pi f$  is the frequency of the field's oscillations.

According to Faraday's law an EMF  $\mathcal{E}$  will be induced in the loop according to  $\mathcal{E} = -\frac{\partial\phi}{\partial t}$ , where  $\phi = Ba$  is the magnetic flux through the loop and  $a$  is the loop's area. Therefore, if the loop is perpendicular to the direct of the field, the EMF will be  $\mathcal{E} = a\omega B_0 \sin(\omega t)$ .

Therefore, we can model the loop as a circuit with a resistor, an inductor, and an alternating voltage source.

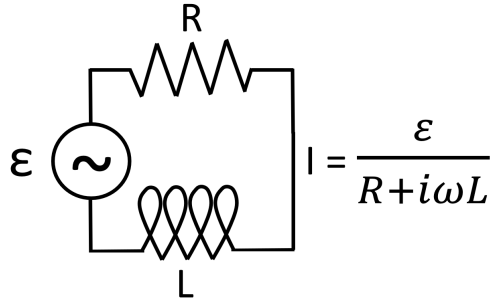


Figure 2.1: Circuit model

Since the circuit consists of both an inductor and a resistor there will be a complex current such that  $I = \frac{\varepsilon}{R + i\omega L}$

### 2.1.2 Magnetic Moment of Conducting Loop

The energy of a magnetic dipole in a magnetic field is given by the interaction Hamiltonian  $H = -\vec{\mu} \cdot B$  [5][4.185], where  $\vec{\mu}$  is the magnetic moment of the dipole, i.e. the induced current loop.

For a flat current loop,  $\vec{\mu} = Ia\hat{n}$  where  $I$  is the current through the loop and  $a$  is the area. So  $H = -Ia\vec{B} \cdot \hat{n}$

The current, as stated above depends on  $\varepsilon$ ,  $R$ ,  $\omega$ , and  $L$ . If the magnetic field is assumed to be  $B = B_0 \cos(\omega t)$ , then the EMF will be  $\varepsilon = B_0 \sin(\omega t)$ . Substituting  $\varepsilon$  into the current equation, and current into the energy equation yields the following:

$$H = -\omega B_0^2 a^2 \frac{\sin(\omega t)}{R + i\omega L} \cos(\omega t) \quad (2.1)$$

In the case where the resistance dominates ( $R \gg \omega L$ ), the energy is

$$H = -\omega B_0^2 a^2 \frac{\sin(\omega t)}{R} \cos(\omega t) \quad (2.2)$$

In the case where inductance dominates ( $\omega L \gg R$ ), the effect of dividing by  $i$  is to shift the sine term 90 degrees out of phase at which point it is identical to a cosine

term.

$$H = \frac{\omega B_0^2 a^2 \cos(\omega t)^2}{\omega L} \quad (2.3)$$

The time average of  $\sin(\omega t)\cos(\omega t)$  is zero, so in the case where resistance dominates the interaction between the magnetic field and the loop averages to zero.

$$\langle H \rangle = 0 \quad (2.4)$$

The time average of  $\cos(\omega t)^2$  is  $\frac{1}{2}$ , so in the case where inductance dominates the interaction between the magnetic field and the loop averages to the following:

$$\langle H \rangle = \frac{1}{2} \frac{a^2 B_0^2}{\omega L} \quad (2.5)$$

In a circuit with both a resistor and an inductor, the significance of each component is dependent on the voltage drop across each component. Voltage drop depends on the impedance of the components, and is higher in a given component if the relative impedance is higher.

Therefore, if the reactance ( $\omega L$ ) due to self-inductance of a conducting loop is significantly greater than the loop's resistance, then the interaction energy, the Hamiltonian, is proportional to the oscillating magnetic field squared. The gradient of the Hamiltonian is the force. Therefore, if there is a spatial dependence to the magnetic field, then the field will exert a force on the loop.

### Inductance of a Torus

Toroidal rings or loops act as self-inductors in a magnetic field.

As stated above, the force effect will occur if reactance is greater than resistance. Reactance depends on the frequency of the magnetic field. The force will occur if and only if  $\omega L > R$

The crossover frequency is the frequency at which inductive reactance is equal to resistance.

$$\omega = \frac{R}{L} \quad (2.6)$$

The self-inductance of a torus in magnetic field, according to research by Mak and Young [1], is as follows, where  $\mu_0$  is the permeability,  $D$  is the diameter of a torus and  $d$  is the cross-sectional diameter:

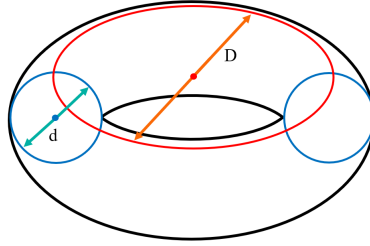


Figure 2.2: Diagram of torus

$$L = \frac{\mu_0 D}{2} \left[ \ln\left(\frac{8D}{d}\right) - \frac{7}{4} \right] \quad (2.7)$$

The resistance of a wire with cross sectional area  $A_{cross-section}$  is as follows where  $\rho$  is the resistivity of the material and  $l$  is the length of the wire:

$$R = \frac{l\rho}{A_{cross-section}} \quad (2.8)$$

For a ring, the cross sectional area is the area of the circle  $\pi \frac{d^2}{4}$ . The length of the ring is  $\pi D$ .

$$R = \frac{4D\rho}{d^2} \quad (2.9)$$

Combining equations 2.7 and 2.8 in the framework of equation 2.6 yields:

$$\omega \left[ \frac{\mu D}{2} \left[ \ln\left(\frac{8D}{d}\right) - \frac{7}{4} \right] \right] > \frac{4\pi D\rho}{\pi d^2} \quad (2.10)$$

Equation 2.10 can be solved for crossover frequency if the material, and the ratio of  $D$  to  $d$  is known. To illustrate, let's use the specifications for the micro rings currently being fabricated by VCU for this project. Those rings are made of aluminum.  $D$  is 50 microns,  $d$  is 16 microns.

In that case, the crossover frequency would be

$$\omega = \frac{R}{L} = \frac{\frac{4D\rho}{d^2}}{\frac{\mu*D}{2} \left[ \ln\left(\frac{8D}{d}\right) - \frac{7}{4} \right]} = 0.489 \text{ Ghz} \quad (2.11)$$

### 2.1.3 Material Quantities

In this subsection I will briefly discuss the dielectric qualities of the substrates used for this project. For this project we are interested in the dielectric constant and loss tangent of the aluminum nitride layer of one of the substrate candidates.

The relative permittivity or dielectric constant  $\epsilon_r$  of a given material is the ratio of the capacitance of a capacitor using that material as a dielectric, with the capacitance of a capacitor using vacuum as a dielectric.

The loss tangent of a material measures the loss of electromagnetic energy, into a material through which it propagates, in the form of heat. The loss tangent is defined as the ratio between the real and imaginary impedance at a given frequency. It can be calculated as follows, where  $\sigma$  is the conductivity,  $\epsilon = \epsilon_r \epsilon_0$  *is the permittivity, and*  $\omega$  is frequency.

$$\tan(\delta) = \frac{\sigma}{\omega\epsilon} \quad (2.12)$$

# Chapter 3

## Macroscopic Experiments

This chapter presents several tests, conducted at centimeter scale, to verify the theory discussed in chapter 2. In section 3.1, an experiment is conducted to measure the force predicted in section 2.1.2. Section 3.2 presents the successful measurement of the crossover frequency of a conducting ring from resistive behavior at low frequencies to inductive behavior at high frequencies.

### 3.1 Ring Force Testing

To measure the strength of the force exerted on the ring, a pendulum with a wire hairpin loop hanging from the end was set next to a wire with an alternating current.

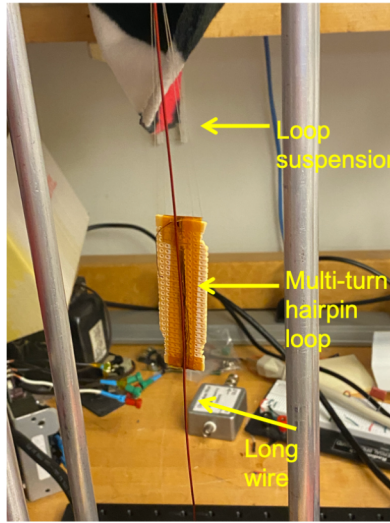


Figure 3.1: Beling's Original Setup

This experimental design was based on the work of Beling (2020) [2] (see figure 3.1), but two crucial changes were made. First, the geometry of the magnetic wire was adjusted to be horizontal instead of vertical (see figure 3.2). This new orientation made it possible to shorten the distance between the wire and the loop relative to Beling's design.



Figure 3.2: Pendulum with Horizontal Wire Geometry

The second change was that the apparatus was isolated from air currents by placing a box around the pendulum (see figure 3.3). Before this change, air current perturbations caused the pendulum to constantly oscillate randomly. After the box was constructed the pendulum was static. To observe the motion of the loop while the box was in place, a camera was installed.



Figure 3.3: Pendulum With Box

Once these changes were in place, the alternating magnetic field was created by running an AC current through the horizontal wire. The frequency was determined by a frequency generator which controlled a current source. The current source was connected directly to the wire. The current was measured in series with a Hall Effect ammeter. The current was approximately 4 amps. The range of the frequency of the field was 700 Hz to 10 kHz. Figure 3.4 shows the electrical apparatus.



Figure 3.4: Cart with Electronics

### 3.1.1 Results

#### Initial Results

No force was observed when the loop was exposed to the magnetic field. The pendulum remained static. The plan was to measure force more precisely after movement was initially observed, but since no movement was observed it was not possible to proceed in that direction.

The causes of this unexpected result were investigated. Ultimately it was determined that the primary problem was that the frequency being used was well below the crossover frequency.

The following steps were taken to reach that conclusion.

## Expected Force

The first possibility considered was that the force on the loop was too small to observe. To determine if that was the case the expected force and expected displacement was calculated using the properties of a hairpin loop.

The force on the hairpin loop is as follows where  $l$  is the length of the loop,  $h$  is the width of the loop,  $d$  is the cross sectional diameter of the loop's wire, and  $s$  is the distance between the loop and the B-field source [2] [3.26].

$$\vec{F} = \frac{\mu_0 I_0^2 \cos(\omega t)^2 (l - 2d)^2 h}{4\pi l \ln(\frac{h-d}{h})} \left[ \frac{h - 2d}{s(s+d)(s+h-d)} + \frac{\ln(\frac{s+h-d}{s+d})}{s^2} \right] \hat{s} \quad (3.1)$$

The expected force on the ring in this setup is approximately  $10^{-4} N$ . Given that the mass of the loop is about 5 grams and the length of the wire about 60 cm, the expected lateral movement given the force is 1.5 mm which should be large enough to see through the camera.

## Measuring Crossover Frequency With Solenoid

Next an attempt was made to measure the cross over frequency directly.

To do this, the loop was placed in a solenoid with an alternating magnetic field. The current inputted into the solenoid, and the loop, were both measured and displayed on an oscilloscope. As described in the theory section, the resistive behaviour will be 90 degrees out of phase with the magnetic field, while the inductive behaviour will be in phase with the magnetic field. As the frequency increases the current going through the loop will gradually move to be in phase with the current going through the solenoid. By adjusting the frequency and determining when the phase shift occurs, the crossover frequency of the inductor can be found.

Unfortunately, no induced voltage was detected in the loop. Making this measurement impossible.

## Calculating Crossover Frequency

Since direct measurement was unworkable, the inductance and resistance were measured using an LCR meter, and the results were used to calculate the crossover frequency according to equation 2.6.

The resistance was  $0.9 \Omega$  and the inductance was found to be  $2.4 \mu\text{H}$ . The crossover frequency was found to be  $370 \text{ kHz}$ .

Because the frequency of the field was much lower than the crossover frequency of the loop, the resistive behavior dominated, explaining why the expected behavior was not observed.

## 3.2 Crossover Frequency Experiment

As discussed in the theory section, it is expected that when an alternating magnetic field induces a current in a loop, the resulting current will be 90 degrees out of phase with the alternating field at low frequencies, and 180 degrees out of phase at high frequencies. To verify this behavior an experiment was conducted to measure the phase relationship between the frequency of the oscillating magnetic field and the frequency of the induced current in the loop.

A alternating magnetic field was generated inside a solenoid. The current through the solenoid was controlled by a frequency generator, allowing the frequency to be adjusted.

Inside the solenoid an inductor loop was placed. Two long wires extended from the loop out of the solenoid, where they connected the loop in series to a  $1 \Omega$  resistor.

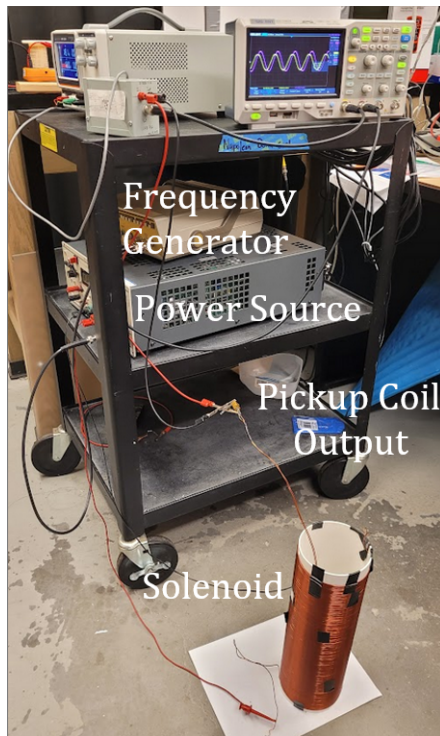


Figure 3.5: Electrical Set Up

The output of the frequency generator, the current through the solenoid, and the inducted current, were all measured by an oscilloscope (see output below in fig. 3.6). As the frequency was adjusted, the difference between the zero points of the solenoid current and the inducted current was measured <sup>1</sup> This difference was used along with the frequency to calculate the phase difference.

---

<sup>1</sup>In an earlier iteration of this experiment the difference between peaks was measured instead, but as it was found that the current plots became more irregular at high frequencies and the exact peak was sometimes hard to determine, it was decided that the zero point was a more reliable measure.

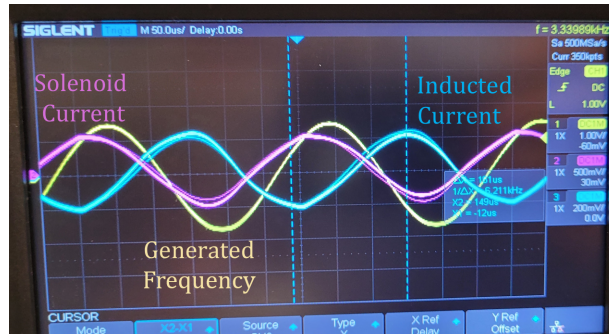


Figure 3.6: Oscilloscope Output

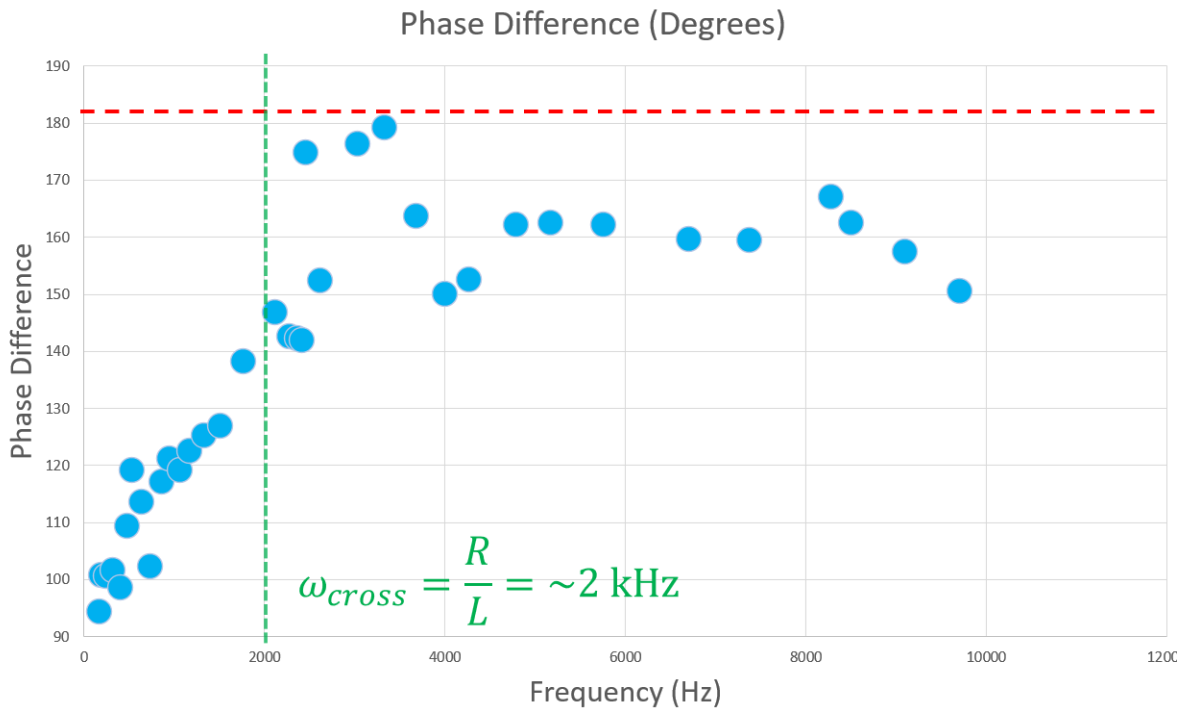


Figure 3.7: Graph of Phase Difference by Frequency

The behavior of the induced current matched theoretical predictions (see figure 3.7). However, while the inflection point of the curve is roughly at the crossover frequency (2kHz) the full 180 degree phase difference does not occur until frequency is significantly higher.

This indicates that the previous model of inducted current behavior, where it

was assumed the behaviour was entirely resistive below the crossover frequency, and entirely reactive above the crossover frequency, is only good as a first order approximation. For the actual microwave tweezer chip production it should be anticipated that the rings will not levitate until the chip is operating at 1.5 to 2 times the crossover frequency of the microrings.

# Chapter 4

## Microwave Tweezer Chip Development

The ultimate goal of this project is to levitate microrings using microwave tweezers [4]. The microwave tweezers will be manufactured in collaboration with VCU. Each substrate consists of a copper layer and an aluminum-nitride layer. On top of the aluminum-nitride layer, copper traces, called microstrips, will be deposited. Table 4.1 shows the target values that had to be met so that this deposition process could be successful. Smoothness is surface bumps, uniformity is center to edge.

To advance this research thrust, substrate candidates were produced and examined. In addition, a microstrip resonator chip was designed to measure the aluminum nitride coatings' dielectric constant and loss tangent.

| Substrate      | Surface Bumps | Center to Edge | Thickness   |
|----------------|---------------|----------------|-------------|
| Target         | <1 micron     | 10 microns     | 50 microns  |
| CERcuits       | 2-3 microns   | 50 microns     | 380 microns |
| Lab Produced   | 1 micron      | 10 microns     | N/A         |
| Nitride Global | < 1 micron    | N/A            | 30 microns  |

Table 4.1: ~~Table 4.1.~~ Substrate Properties

## 4.1 Atom Chip Substrate Candidate

The first substrate this paper will discuss was intended for use with the atom chip, unlike the other two which are both intended for use with the microwave tweezer chip.

As mentioned in the motivation section, the principles and procedures for developing the microwave tweezers will be modified and replicated by the William & Mary ultracold atom lab. The atom chip requires a much thinner substrate. One of the candidates was a thin copper sheet, coated on one side with a layer of aluminum-nitride purchased from CERcuit 



Figure 4.1: Both Sides of CERcuits Substrate Candidate

To determine if this product would be a good candidate for the atom-chip, its planarity and smoothness were tested by measuring it with the same DEKTAK machine used to scan the copper plates.

A map scan was run across the copper side of the sample to assess the planarity of the sample and the smoothness of the copper . After that step was complete, another scan was run on a smaller patch at the center of the aluminum-nitride side of the sample to assess the smoothness of the aluminum-nitride layer .

The sample was curved inwards. The variation between the lowest point, in the center of the sample, and the highest point in the corners, was  $162.9 \mu\text{m}$

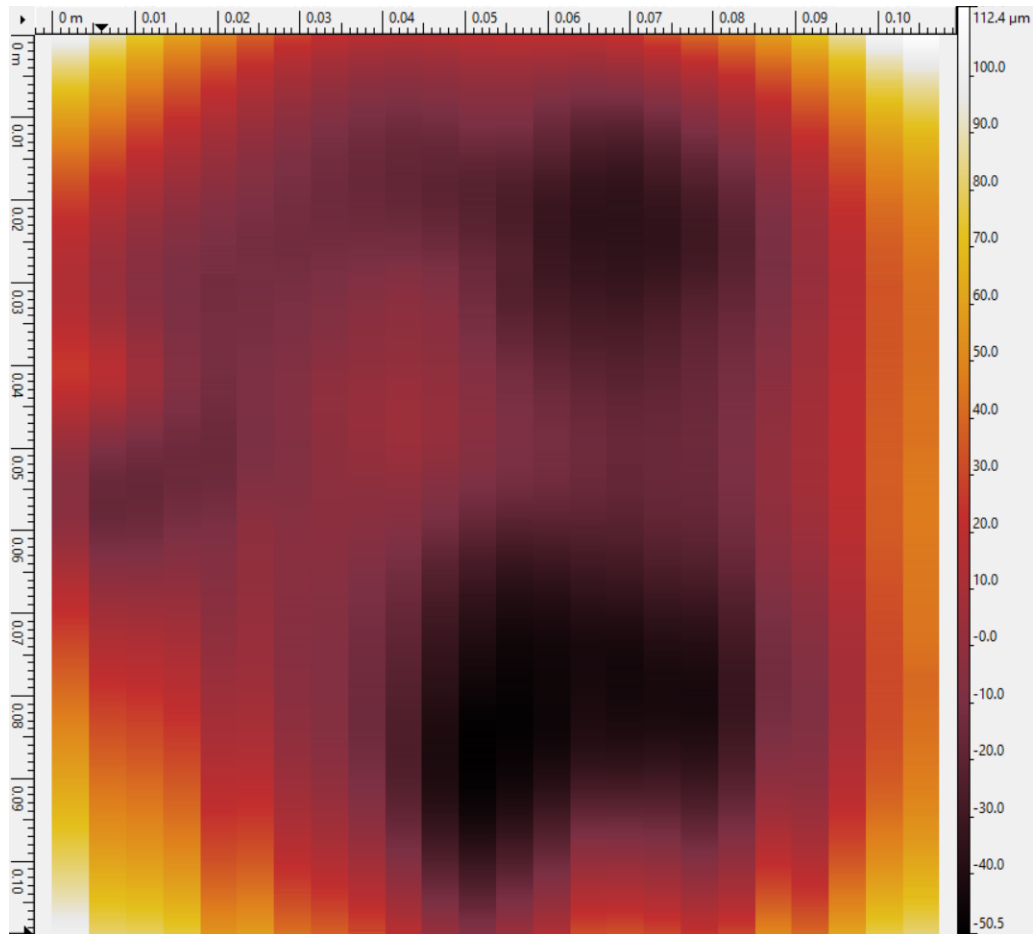


Figure 4.2: DEKTAK map of Copper Side 

To determine the smoothness of copper side of sample the variation in height over a line was graphed. The average value of variation in this sample was on the order of 1-2 microns.

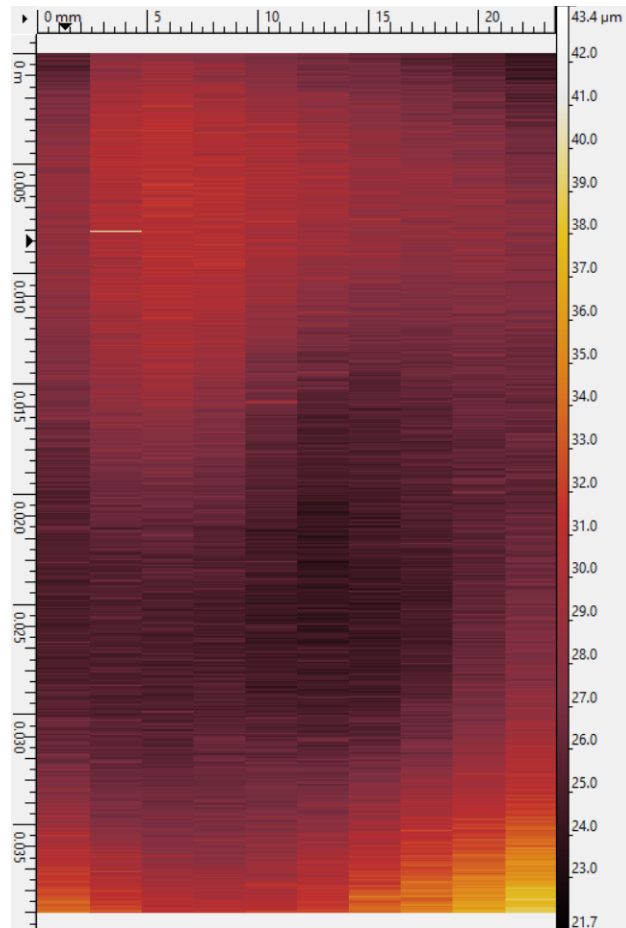


Figure 4.3: DEKTAK map of Aluminum-Nitride S1 

The above process was repeated with the aluminum nitride side. The average value of variation in this sample was on the order of 2-3 microns.

Smaller scans were then taken of each side to determine where the variations were small spikes or large patches . It was hoped that large patches would not disturb the additive manufacturing process.

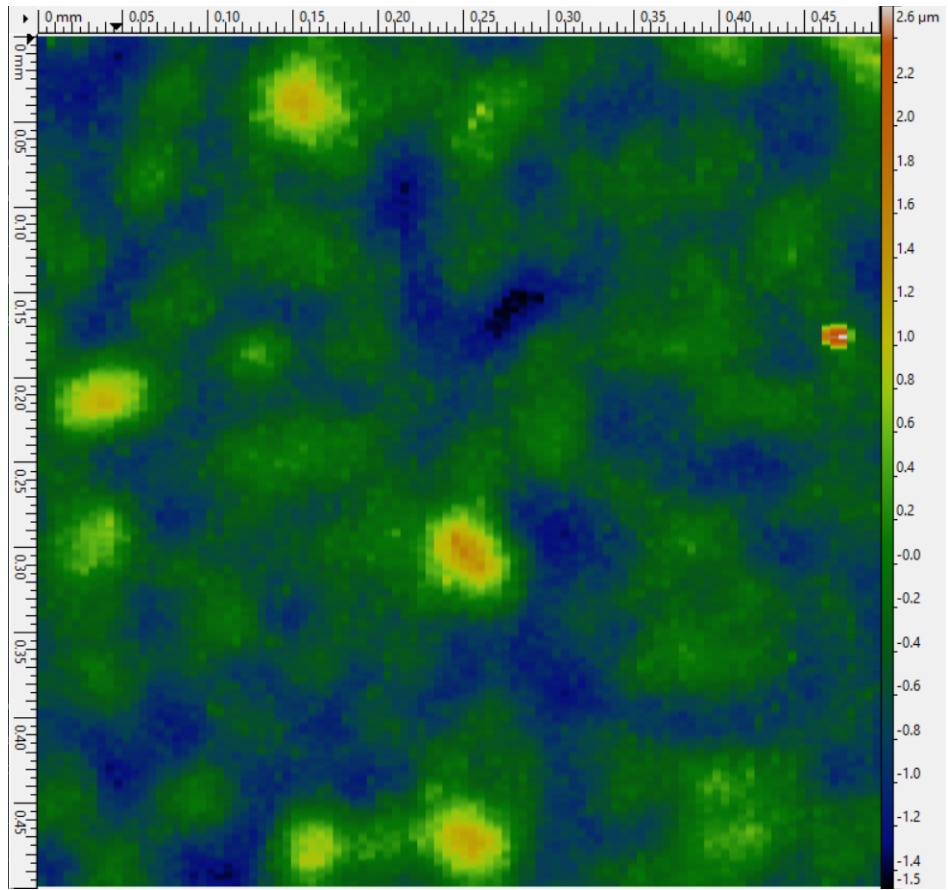


Figure 4.4: Precise DEKTAK map of Copper Side 

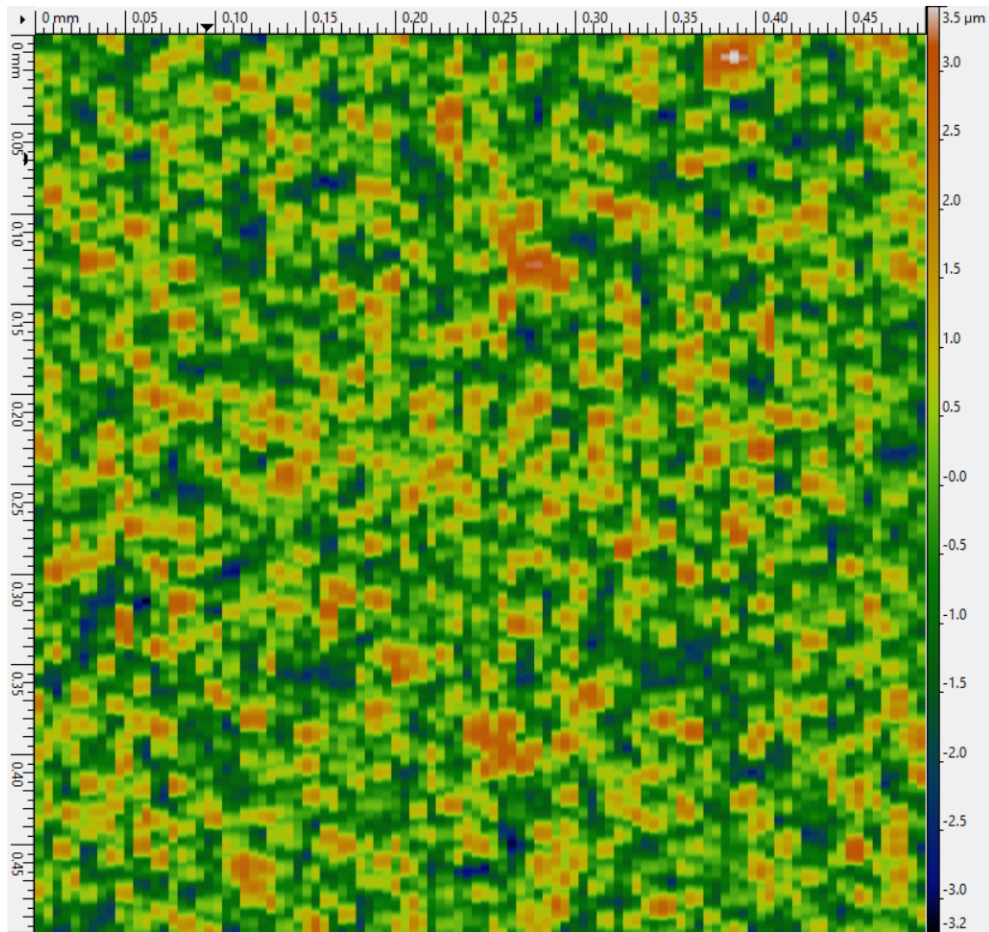


Figure 4.5: Precise DEKTAK map of Aluminum-Nitride Si 

As can be seen in figure 4 , the variations in the aluminum nitride were spikes not patches, and were too dense for the microstrips to avoid.

Ultimately it was determined that, because of the roughness of the the aluminum nitride side, this substrate was unsuitable for the atom chip.

## 4.2 Microwave Tweezer Substrate Candidate One

### 4.2.1 Purpose and Requirements

As stated above, the microwave tweezer chip will be built on top of a copper substrate. The process of coating and microtrace deposition requires uniformity. Ergo, the

substrate must be very flat and have no scratches deeper than 1  $\mu\text{m}$ .

One option to manufacture a substrate was to cut commercial copper and manually polish the pieces until they met the required specifications.

### **Manufacturing Procedure**

The substrates were cut out of copper sheets into 3 cm x 3 cm squares and 5 cm x 5 cm squares, each with a thickness of about 2.1 mm. When initially cut they did not meet required specifications flatness nor smoothness.

To flatten the substrates and to remove scratches, the polishing procedure outlined in Beling 2021 were followed [2]. Each plate was polished by being rubbed against sandpaper which was laid across a highly planar granite working surface. Plates were rubbed across the sandpaper in figure eight patterns or alternating clockwise and counterclockwise circles. The grit of sandpaper used was progressively increased. The grits used were P220, P240, P320, P400, P600, P1000, P1200, P1500, P2000, P2500, P5000, and P7000.



Figure 4.6: Copper Plate Before and After Polishing

After each grit of sandpaper was applied, the plates were inspected to determine if any scratches had been revealed by the latest grit. If there were scratches and they were too deep for the current grit to remove in a timely manner, the process would start again at the previous grit of sand paper.

## Testing Finished Substrates

The properties of the material were tested via the Applied Research Center Core Lab's DEKTAK Profilometer. The DEKTAK measures the surface profile of a material by dragging a very small needle across its surface.

A map scan was run across the substrates. The map scan produced an image recording the topography of the surface of each plate with a resolution of 1.5 mm horizontally and 1 micron vertically. The scans were analyzed in the program Gwyddion. In Gwyddion the scans were rectified to account for the tilt of the machine, and when analyzing smoothness, the polynomial shape of the reduced edges. If the substrate fit the required parameters, it was sent to VCU to begin the next phase of manufacture.

The copper plates were all within required parameters for flatness and smoothness. The below scan shows how the sample was slightly convex, varying by about 10  $\mu\text{m}$ .

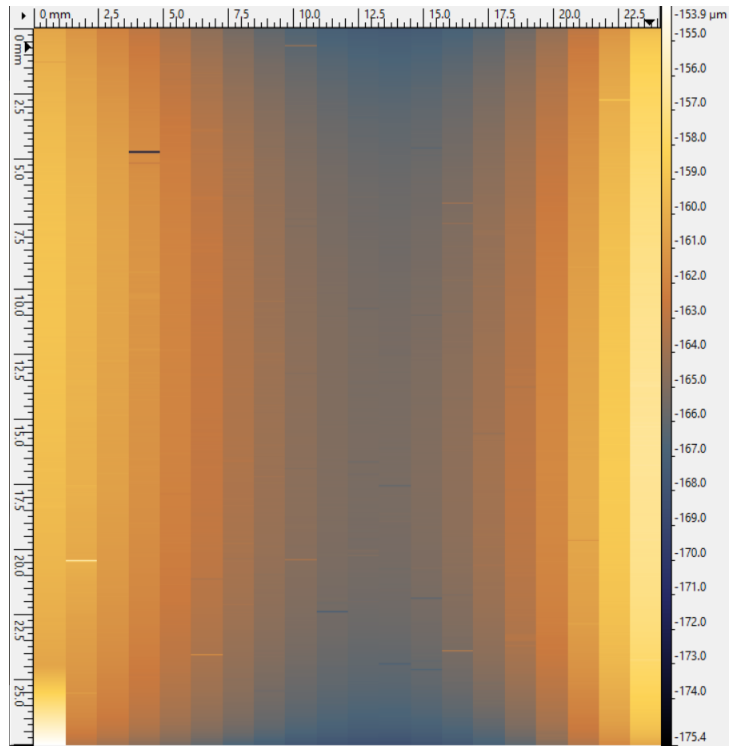


Figure 4.7: DEKTAK map of Copper Plate Planarity

The plate had scratches on the order of 1-2  $\mu\text{m}$ , well within parameters. There was one exception, a small pit about 13  $\mu\text{m}$  deep. Since this was small pit instead of a scratch across the entire surface, this flaw was determined to not compromise the substrate because unlike a normal scratch which is across the whole surface, it was extremely localized and thus can be easily avoided during the additive manufacturing process.

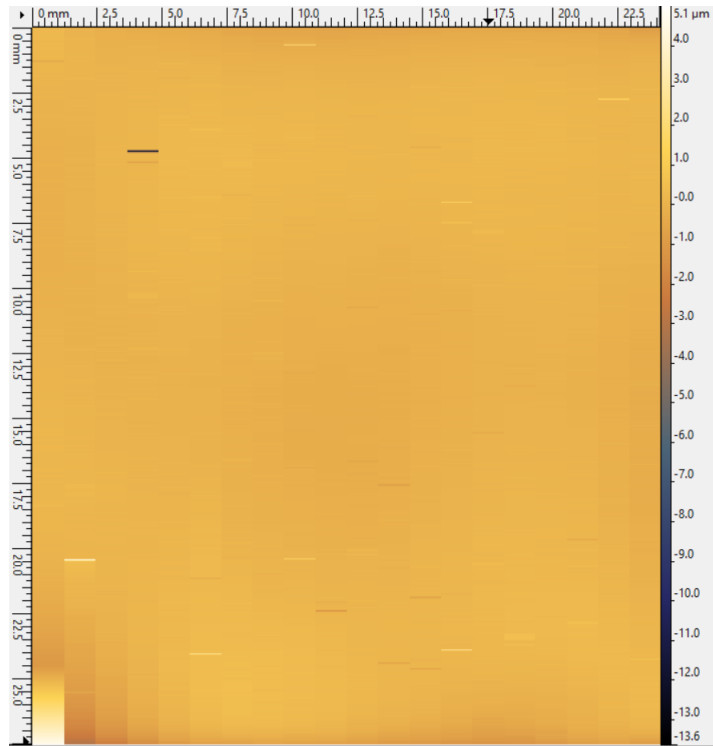


Figure 4.8: DEKTAK map of Copper Plate Smoothness

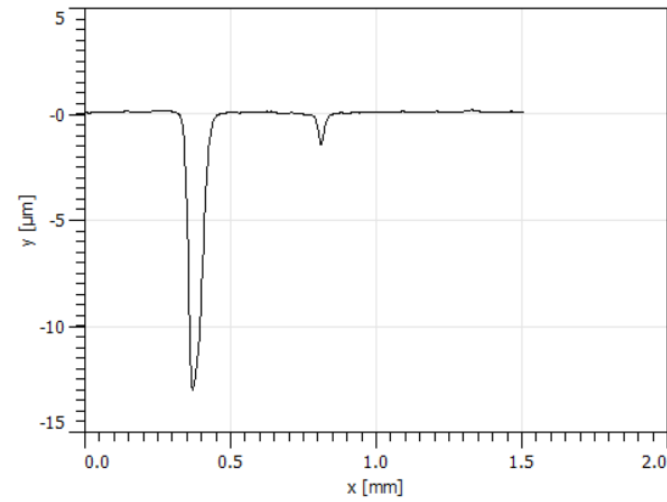


Figure 4.9: DEKTAK Profile Along Line Showing Anomaly

The above profile was taken across the dark spot on Figure 4.8.

Unfortunately, for the last 5 substrates, the DEKTAK was no longer available.

Instead the the Applied Research Center Core Lab's optical profilometer was used. Unlike the DEKTAK the optical profilometer could not take a map scan and was limited to scanning 1 mm x 1 mm patches. A sample of three patches per substrate were scanned, focusing on the most visible scratches. Once again there were no scratches deeper than 5 microns so the sample was sent to VCU .

#### **4.2.2 Grit Polishing and Testing**

At VCU more testing was conducted and a final stage of polishing was conducted. This was done by putting the samples in a bath including an abrasive diamond grit and oscillating the bath.

It was intended that the samples would be shipped to a third party company to have an aluminum nitride coating applied, but first one last round of measurements were conducted which disrupted this plan.

The samples were measured using the William & Mary Applied Research Center Core Labs' optical microscope, the Hirox. When this was done it was discovered that there were dark patches left on the surface of the substrate.

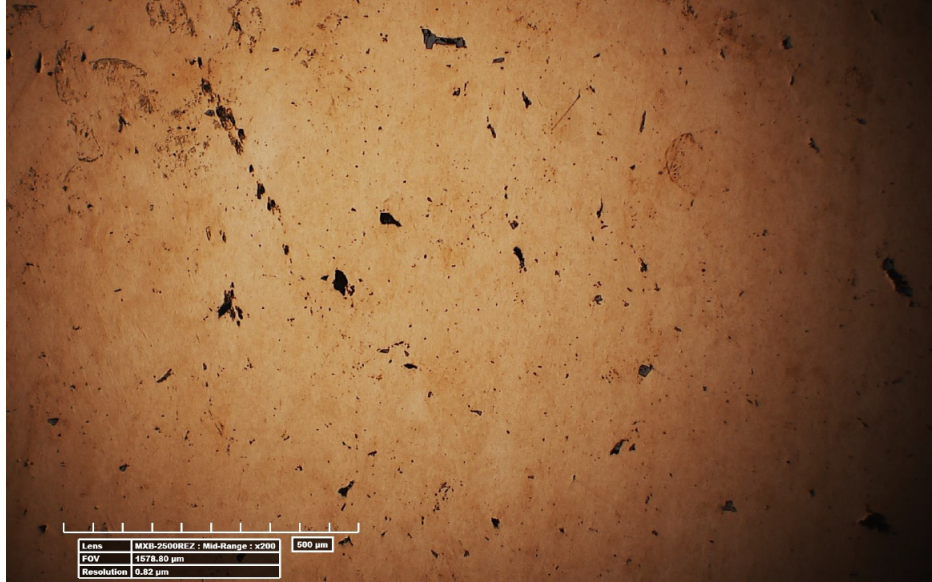


Figure 4.10: Optical Scan of Substrate (Magnification = 200x)

It is hypothesized that these black patches were residue from the diamond grit used in the final polishing process. While the samples were not scanned with the Hirox until after the final polishing process, they were scanned with the Dektak and we'd expect these patches to show up in the Dektak scans.

These patches were problematic for continued substrate development because of the high probability they contained carbon from the diamond grit. Carbon is problematic because even in small amounts it can disrupt the nitride deposition process.

### 4.2.3 Attempted Cleaning and Testing

An attempt was made to remove the black patches from the samples. To test if the process would work, a sample was placed in a bath of distilled water and alconox detergent. An ultrasonic bath was then applied over a period of 12 hours to "scrub" the surface. After this process the surface was rinsed with methanol.

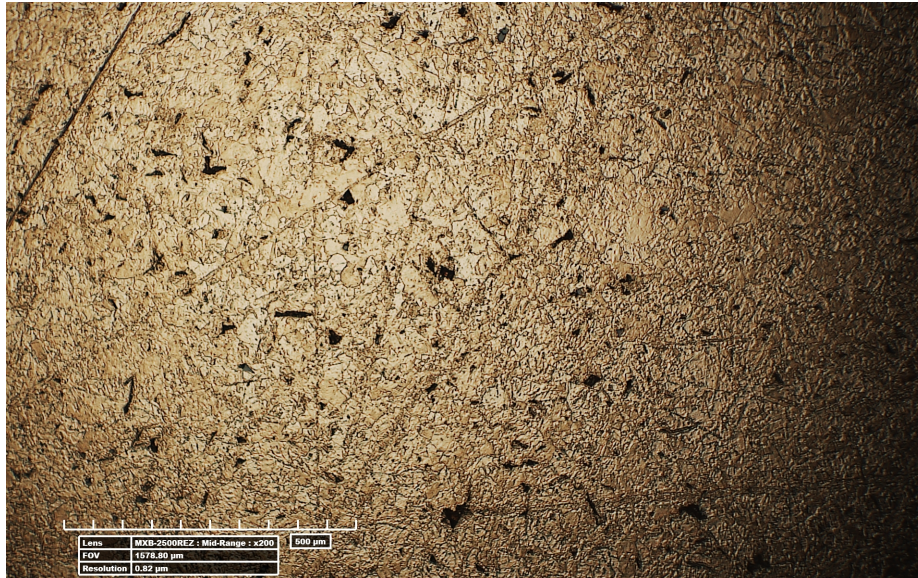


Figure 4.11: Optical Scan of Substrate After Cleaning (Magnification = 200x)

After the cleaning process the substrate was again examined with the Hirox. It was found that the surface looked much rougher than before, and the black patches, while somewhat reduced, were not gone entirely.

It was concluded that this substrate candidate was no longer viable for the microwave tweezer chip due to the risk of a low quality aluminum-nitride coating.

#### 4.2.4 Future Work

If more copper substrates are needed matching these specifications, this process can potentially still be employed, but the final stage of grit polishing should be skipped. After manual polishing, future researchers should use the Hirox to verify that the black patches are not present before grit polishing. Another potential avenue of useful research would be to use the SEM's element identification function (discussed further in next section) to verify that the patches are carbon. If they are not, then it is possible that the substrates might be of use. Finally, future researchers may wish to examine if there are other methods of cleaning that would be more successful.

## 4.3 Microwave Tweezer Substrate Candidate Two

Another substrate candidate were samples produced by Nitride Global LLC. Nitride Global provided four samples each consisting of a copper substrate (with a thickness of 1 mm) and an aluminum nitride coating (with a thickness of 30  $\mu\text{m}$ ). One of the samples was a narrow strip, two were 27 mm  $\times$  37 mm, and one was 37 mm  $\times$  37 mm. Later, another batch was received of 20 samples each with an aluminum nitride thickness of 20 microns. This AlN thickness is below the requirements for both the microwave tweezer chip and the atom chip, so that later batch of samples will instead be used to refine the manufacturing process.

The coating was not quite pure aluminum nitride. For that reason, the exact properties of the material are unknown as it should be slightly different from pure aluminum nitride.

The copper substrate was manufactured by another third party, possibly via electropolishing. As verified in the DEKTAK, it was well within required specifications for flatness.

### 4.3.1 Measuring Thickness With Optical Microscope

The next step was to determine the exact thickness of the aluminum nitride layer. While the manufacturer listed 30 microns as the intended thickness, it was decided that more precise measurements should be made. The properties of the any chip made with the substrate depends on the exact AlN thickness so a precise measurement was needed before the design process could begin.

The first plan was to examine one of the edges of the sample under the Hirox optical microscope. This was made difficult because the AlN layer was transparent. It was hoped that despite the transparency, the AlN layer would be visible and easily measured when magnified.

A device was constructed to hold the samples upright without applying pressure to the aluminum nitride coated surface. The device accomplished this by holding the substrate samples by their edges between two strips of sorbothane foam. The distance between the strips was controlled by a Thorlabs manual translating stage.



Figure 4.12: Substrate Holder

Unfortunately the images were not as useful as hoped. The boundaries of the AlN layer were not clear. It was not even clear if the AlN layer was visible at all. In figure 4.8, the right hand edge of the substrate, where the aluminum nitride coating is, does not have a clear boundary.

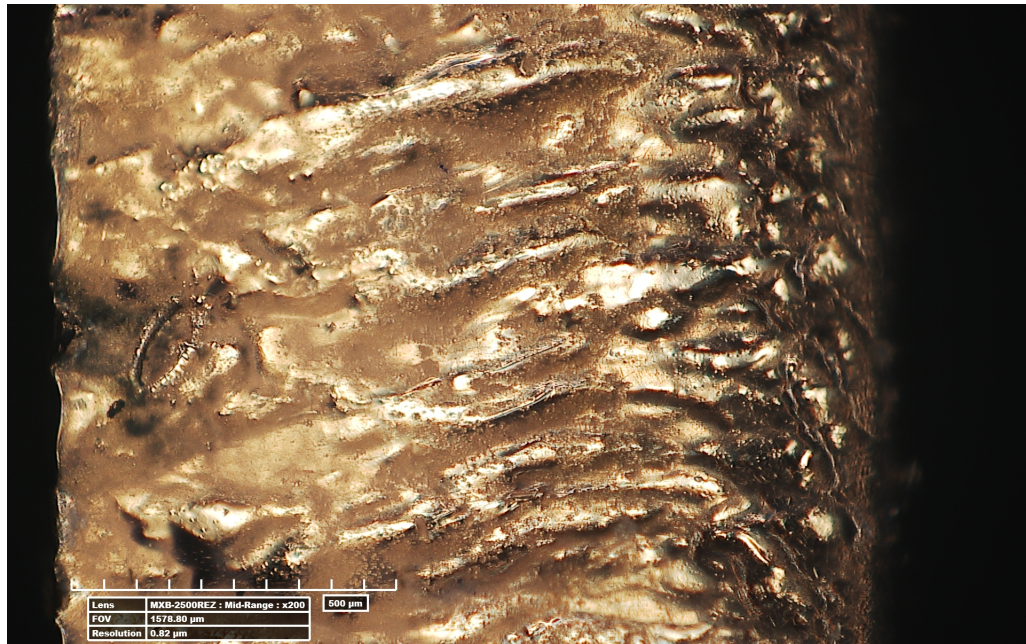


Figure 4.13: Substrate Edge

Next another attempt was made to determine thickness by observing the substrate under the Hirox while a laser was incident on its surface. It was hoped that the laser would illuminate the transparent AlN layer. In the below image it was observed that there did indeed appear to be a transparent layer on the substrate's surface. After analyzing the images it was concluded that the thickness of the layer was indeed about 30 microns, but further testing was needed to find a precise thickness.

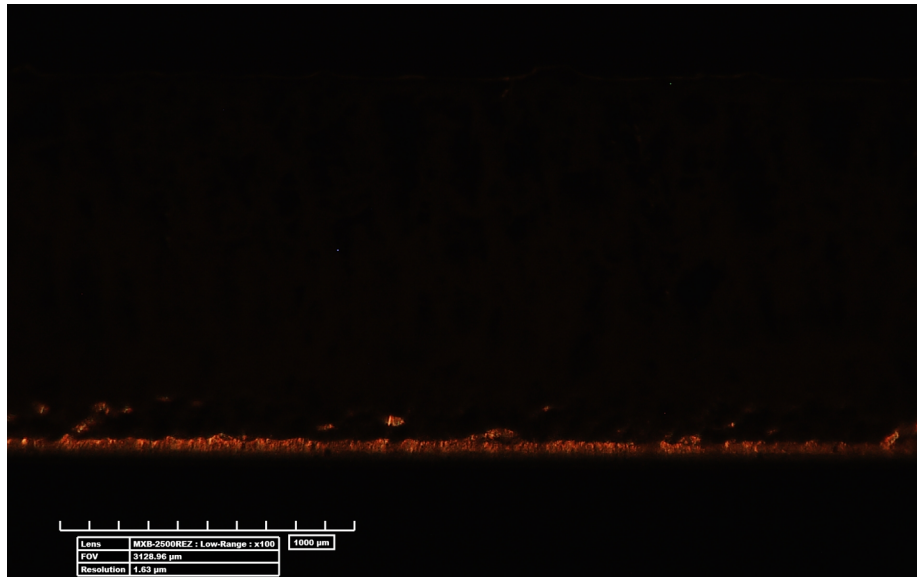


Figure 4.14: Laser Image 

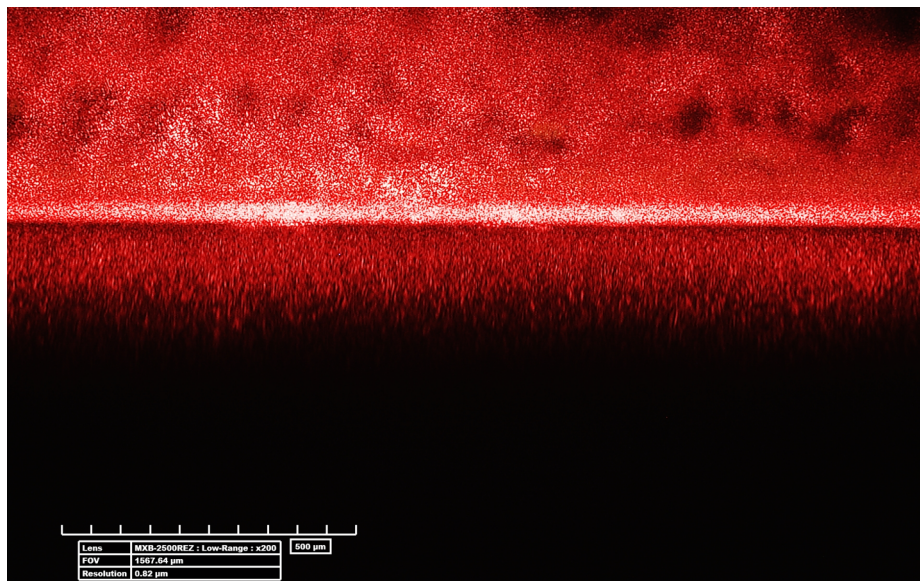


Figure 4.15: Laser Image 

### 4.3.2 Measuring Thickness With SEM

Next a scanning electron microscope was used to obtain a more precise measurement. To obtain a clear cross section image of the edge of the substrate, it was necessary to

first remove the AlN coating on the edge. This was done by rubbing the edge with 5000 grit sand paper which had been dampened with methanol.

After this was done, the sample was loaded into the SEM and scanned. Images were saved so that the thickness of the AlN boundary could be determined. In addition the SEM element identification system was used to verify the content of the boundary layer.

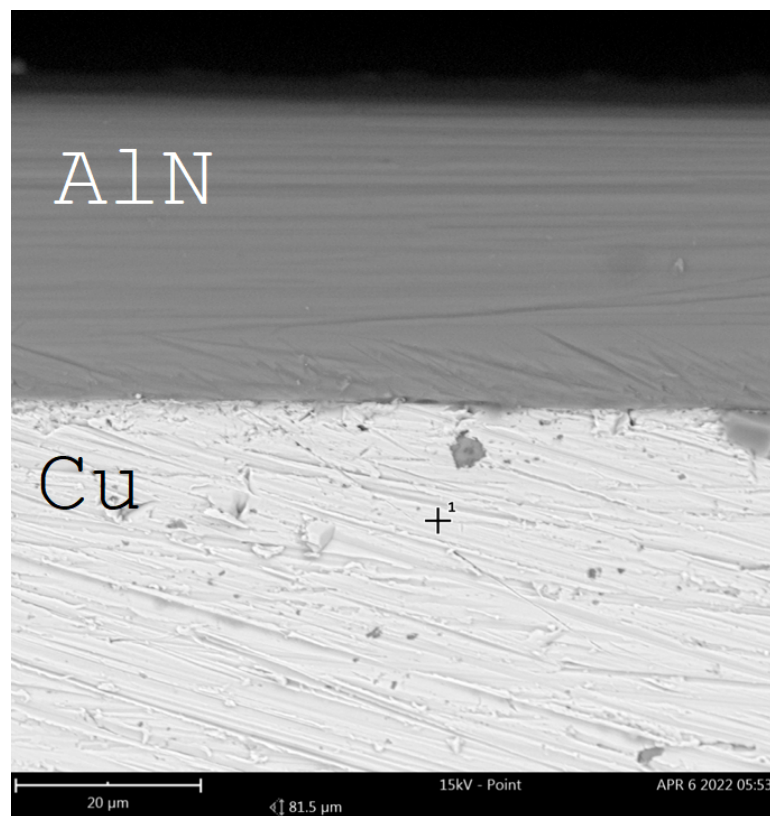


Figure 4.16: Scanning Electron Microscope Image

In the first SEM image there is a shiny pale area which is consistent with the thick copper substrate and a dark gray layer which is consistent with the AlN layer. This is confirmed by the element identification system which identifies copper in the suspected copper area and aluminum, and nitrogen, in the suspected AlN layer.

After analyzing this and 5 other images it was determined that the aluminum

nitride layer has a thickness of 32 microns. This is the measurement used in simulations.

| Scale ( $\mu m$ ) | Scale Length | AlN Length | AlN Thickness ( $\mu m$ ) | Reliability (0-3) |
|-------------------|--------------|------------|---------------------------|-------------------|
| 30                | 6.3          | 6.8        | 32.38095238               | 3                 |
| 30                | 6.3          | 6.7        | 31.9047619                | 3                 |
| 50                | 4.45         | 3.3        | 37.07865169               | 1                 |
| 50                | 4.45         | 3.4        | 38.20224719               | 0                 |
| 50                | 4.45         | 3.2        | 35.95505618               | 1                 |
| 50                | 4.45         | 3.6        | 40.4494382                | 2                 |
| 50                | 4.45         | 3.4        | 38.20224719               | 2                 |
| 50                | 4.45         | 3.3        | 37.07865169               | 2                 |
| 50                | 4.45         | 3.5        | 39.3258427                | 2                 |
| 50                | 4.45         | 3          | 33.70786517               | 3                 |
| 50                | 4.45         | 3.1        | 34.83146067               | 2                 |
| 50                | 4.45         | 2.9        | 32.58426966               | 3                 |
| 50                | 4.45         | 2.9        | 32.58426966               | 2                 |
| 50                | 4.45         | 3.15       | 35.39325843               | 2                 |
| 200               | 5.9          | 0.95       | 32.20338983               | 3                 |
| 200               | 5.9          | 0.9        | 30.50847458               | 3                 |
| 200               | 5.9          | 0.9        | 30.50847458               | 3                 |
| 200               | 5.9          | 1          | 33.89830508               | 2                 |
| 20                | 5.1          | 8.3        | 32.54901961               | 3                 |
| 20                | 5.2          | 8.3        | 31.92307692               | 3                 |
| 30                | 5            | 5.4        | 32.4                      | 3                 |
| 30                | 5.9          | 6.3        | 32.03389831               | 3                 |
| 30                | 5.9          | 6.9        | 35.08474576               | 2                 |
| 30                | 5            | 5.4        | 32.4                      | 3                 |
| 30                | 5            | 5.3        | 31.8                      | 3                 |
| 30                | 5            | 5.2        | 31.2                      | 3                 |
| 30                | 5            | 5.3        | 31.8                      | 3                 |
| 30                | 5            | 5.25       | 31.5                      | 3                 |

Table 4.2: ~~Table 4.2~~ Measured AlN Thickness

David Pate, one of our partners at VCU, used a Filmetrics film-thickness measurement system to measure the thickness of two other samples. He concluded that the samples had an AlN layer thickness of 30.62-30.83 microns and 30.67-30.95 microns.

## 4.4 Microstrip Design and Simulation

The next step in microwave tweezer chip development will be determining the precise properties of the aluminum nitride layer, including the loss tangent. To find the loss tangent, another chip will be need to be made. The design process of said chip is covered in this section.

To test the loss tangent, a reflective cavity will be created along a microstrip. In the case where the impedance changes across a boundary, a portion of the signal will be reflected according to  $R = \frac{Z_2 - Z_1}{Z_1 + Z_2}$ .  The larger the change in impedance, the larger the reflection. However, in a cavity where there are two reflections, at certain frequencies a standing wave will form, destructively interfering with itself to destroy its own reflection inside the cavity, and constructively interfering to create a transmission escaping the cavity. This is useful to us, because when the reflection spikes to zero, the width of the reflection spikes depend on the dielectric loss and the distance between spikes depends on the dielectric constant.

Several designs were created and simulated using the software Sonnet. All the below designs assumed the metal layer was silver 5 microns thick. The AlN substrate was assumed to be 32 microns thick.

### 4.4.1 Microstrip With Gaps

 The first design tried was a simple microstrip with 2 gaps in the middle. Different lengths were used for the gaps, ranging from 100 microns to 0.5 microns. The trace itself was 25 microns wide. This was chosen because it best achieved an impedance of 50  $\Omega$ .

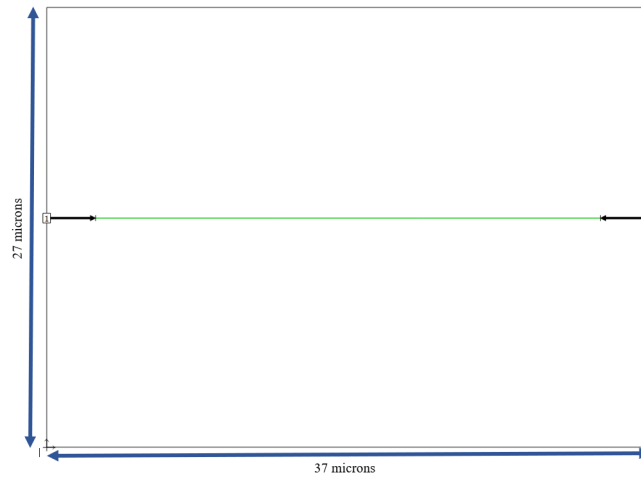


Figure 4.17: One Micron Gaps - Circuit

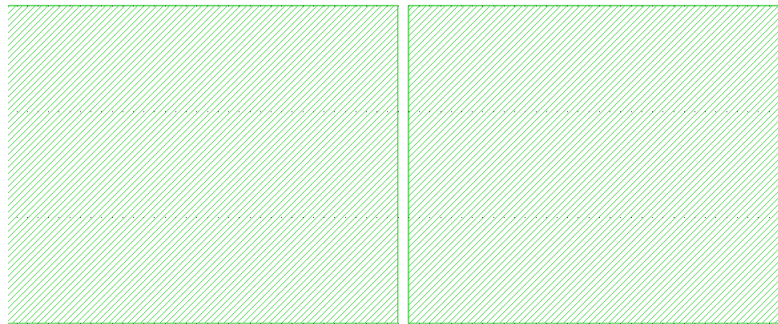


Figure 4.18: Microstrip Resonator with 1 Micron Gaps - Close Up

As can be seen in figure 4.16, the breaks did not have the desired effect. The gaps were too effective at stopping the signal. The transmission behaviour never occurred. As a result, it is not viable to use this design to measure the loss tangent.

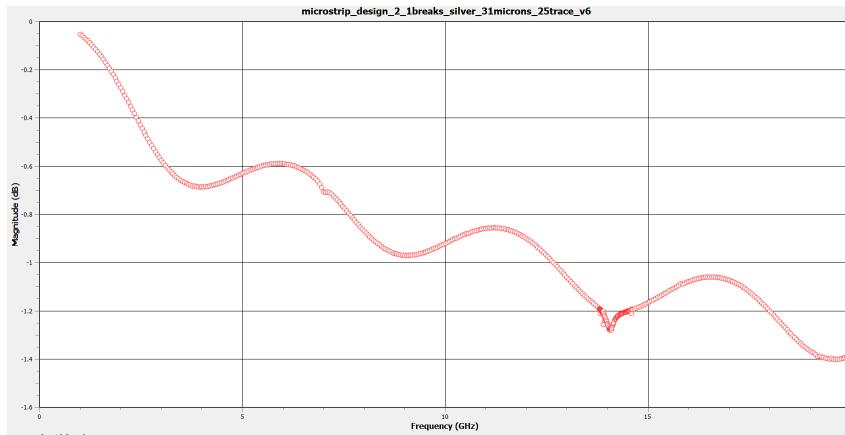


Figure 4.19: Microstrip Resonator with 1 Micron Break - Reflection Graph

#### 4.4.2 Microstrip With Extra Wide Cavity

After the gaps based design failed, a new design was created where the microtrace was 25 microns wide, except for a region in the middle where the trace was suddenly wide . At the boundary between the normal trace and the wider trace there is a significant change in impedance causing a reflection. Different widths were used for this region, ranging from 50 microns to 1025 microns. Ultimately it was decided that the 1025 micron design worked best.

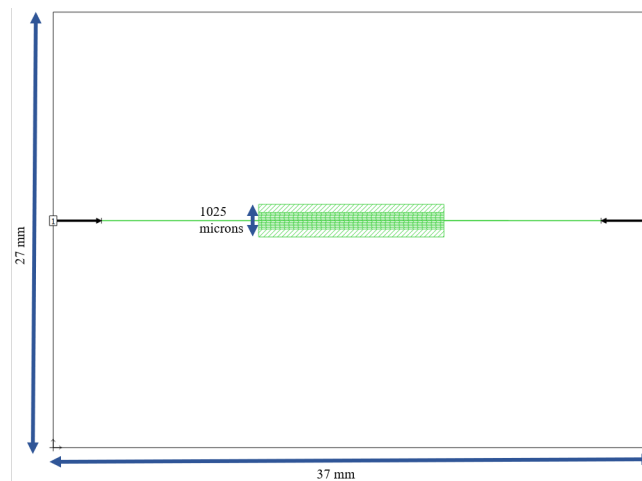


Figure 4.20: Microstrip Resonator With 1025 Micron Cavity - Circuit

As can be seen in figure 40, the design worked as expected. The reflection coefficient was very high except for at the frequencies where standing waves could form. This is the design that the VCU team will manufacture.

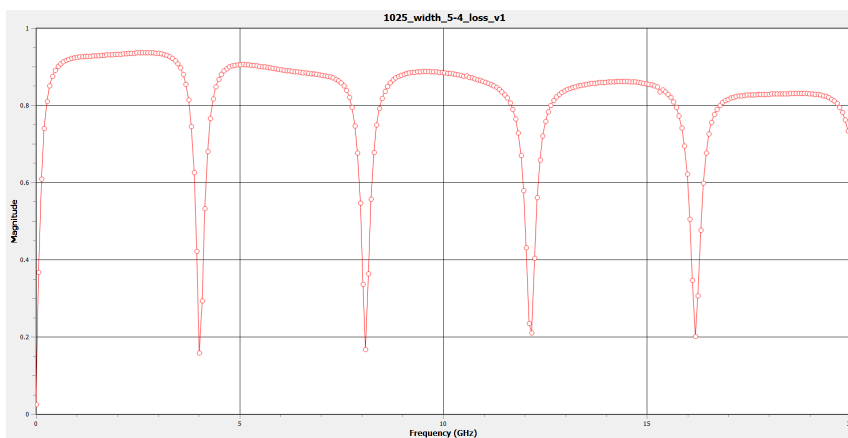


Figure 4.21: Microstrip Resonator With 1025 Micron Cavity - Reflection Graph

As can be seen in figure 41, the shape of the frequency-reflection graph varies with the loss tangent. While the frequency-reflection graphs converge as the loss-tangent approaches zero, this should still be a use full technique for determining an upper bound for the loss tangent.

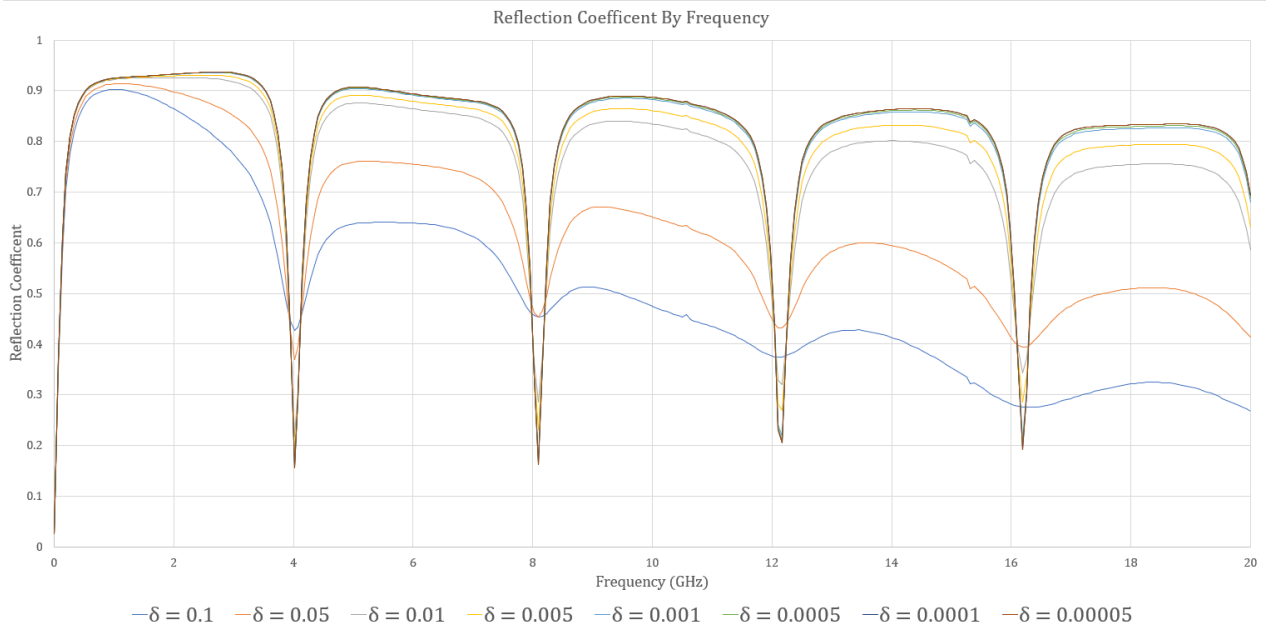


Figure 4.22: Reflection By Frequency for Different Loss Tangents

# Chapter 5

## Summary and Outlook

### 5.1 Summary of Results

This project advanced the microwave tweezer concept through two parallel paths. Experiments with macroscopic objects were conducted to verify theory. At the same time, three candidate substrates were analyzed to determine suitability for the microwave tweezer chip.

For the macroscopic experiments, an attempt to use a pendulum to measure the force of an alternating magnetic field on a loop was unsuccessful. While the test did not produce a useful measurement, it demonstrates the importance of ensuring that the operating frequency of any future microwave tweezer chip is above the crossover frequency of the object the chip is trying to manipulate.

Another macroscopic experiment successfully demonstrated that the phase difference between induced current and the oscillating magnetic field approaches 180 degrees as the field frequency increases above the crossover frequency. This should give us confidence in the theory behind the microwave tweezers and assure us that the microwave tweezers will function at high frequencies. This also tells us that for the best results the operating frequency of the microwave tweezer chip will have to be 1.5-2 times greater than the crossover frequency.

For substrate development, one candidate was produced and two were acquired from a third party. All three candidates were tested, and it was determined that the third substrate candidate was the most suitable for the microwave tweezer chip. The third candidate was also tested to determine the thickness of its AlN layer, and a microstrip resonator was designed to find its dielectric properties. These quantities will be essential for finalizing the microwave tweezer design.

## **5.2 Microwave Tweezer Manufacturing**

The next step is to create the microstrip cavity chip for the loss tangent measurement. This will be done by the VCU team using photo lithography. Once the microstrip cavity chip is manufactured the loss tangent measurement tests will be conducted.

After these experiments the next step will be the manufacturing of the magnetic microwave tweezer chip. Once the microwave tweezers are complete, an experiment will be conducted to levitate aluminum microrings.

# Bibliography

- [1] Mak, SY and Young, K, *Determination of the Self Inductance of a Metal Ring - 1986, Chinese University of Hong Kong.*
- [2] Beling, Andrew John. “Progress Towards Electromagnetic Manipulation and Trapping of Micro-Particles,” 2021,
- [3] Kossler, W. J., Susann Klein, Dominick Morrow, and Andre Juliao. “A Simple Cavendish Experimental Apparatus.” *American Journal of Physics* 84, no. 3 (March 2016): 234–39. <https://doi.org/10.1119/1.4939048>.
- [4] Aubin, S and Avrutin, V. ”Microwave Tweezers for Microfluidic Manipulation.” VMEC Seed Grand Proposal (2019)
- [5] Griffiths, David J. *Introduction to Electrodynamics*. 4th edition. Cambridge, United Kingdom; New York, NY: Cambridge University Press, 2017.